

# Vortex arrays in neutral trapped Fermi gases through the BCS–BEC crossover

S. Simonucci,<sup>1,2</sup> P. Pieri,<sup>1</sup> and G. Calvanese Strinati<sup>1,2</sup>

<sup>1</sup>*Division of Physics, School of Science and Technology  
Università di Camerino, 62032 Camerino (MC), Italy*

<sup>2</sup>*INFN, Sezione di Perugia, 06123 Perugia (PG), Italy*

## Numerical solution of the LPDA equation

We describe the numerical procedure that we have adopted in the main text to solve the LPDA equation for the gap parameter  $\Delta(\mathbf{r})$  (cf. Eq. (2) of the main text), together with the number equation  $N = \int d\mathbf{r} n(\mathbf{r})$  (with  $n(\mathbf{r})$  given by Eq. (6) of the main text) to determine the chemical potential  $\mu$  for fixed particle number  $N$ .

The LPDA equation can be rewritten in the form:

$$\nabla^2 \Delta(\mathbf{r}) + \frac{\tilde{\mathcal{I}}_0(\mathbf{r})}{\mathcal{I}_1(\mathbf{r})} \Delta(\mathbf{r}) - 4miv_n(\mathbf{r}) \cdot \nabla \Delta(\mathbf{r}) = 0, \quad (1)$$

where  $\tilde{\mathcal{I}}_0(\mathbf{r}) \equiv [m^2/(\pi a_F) + \mathcal{I}_0(\mathbf{r})]$  and with  $\hbar = 1$ . The coefficients  $\mathcal{I}_0(\mathbf{r})$  and  $\mathcal{I}_1(\mathbf{r})$  are defined by Eqs. (3) and (4) of the main text. The differential equation (1) is solved over a finite box, with the condition that  $\Delta(\mathbf{r})$  vanishes identically from the boundary of the box outwards. For the trap of ref. [1] the box width is taken as  $2.7R_F$  along the  $x$  and  $y$  directions and  $6.8R_F$  along the  $z$  direction; for the trap of ref. [2] the corresponding widths are  $1.5R_F$  and  $22R_F$ . In this way, the box is at least 1.5 times larger than the size of the cloud in each direction for all rotation frequencies that we have considered.

The differential equation (1) is transformed into a set of finite-difference equations which we schematize in vector form as  $\vec{F}(\vec{\Delta}) = 0$ , by discretizing it over a uniform spatial grid. Here,  $\vec{\Delta}$  is a vector formed by the unknown variables  $\Delta_j \equiv \Delta(\mathbf{r}_j)$  where  $\mathbf{r}_j$  is a point on the grid, while the equation  $F_i = 0$  corresponds to the finite difference version of Eq. (1) at position  $\mathbf{r}_i$ . For the trap of ref. [1] the grid is taken  $800 \times 800 \times 30$  for the  $x, y$ , and  $z$  directions, respectively; while for the trap of ref. [2] the grid is taken  $500 \times 500 \times 50$ . One is thus left with solving a system of  $N_p \simeq 2 \times 10^7$  non-linear equations for the  $N_p$  complex variables  $\Delta_j$ , where the non-linearity arises from the functional dependence of the coefficients  $\mathcal{I}_0(\mathbf{r})$  and  $\mathcal{I}_1(\mathbf{r})$  on  $\Delta(\mathbf{r})$  (cf. Eqs. (3) and (4) of the main text). To solve this system we have implemented a quasi-Newton method as follows. The ordinary (multi-dimensional) Newton method would imply modifying  $\vec{\Delta}$  as follows:

$$\vec{\Delta}^{\text{new}} = \vec{\Delta}^{\text{old}} - \mathbf{J}^{-1} \cdot \vec{F}(\vec{\Delta}^{\text{old}}) \quad (2)$$

where  $\mathbf{J}^{-1}$  is the inverse of the Jacobian matrix  $\mathbf{J}$  with matrix elements  $J_{ij} = \frac{\partial F_i(\vec{\Delta}^{\text{old}})}{\partial \Delta_j}$ . Here, the Jacobian matrix can be calculated quite accurately with a numerical

effort comparable to that of evaluating  $\vec{F}(\vec{\Delta})$ , because most of the off-diagonal elements vanish and those different from zero are linear combinations of  $\Delta_i$  and  $\Delta_j$ . The memory storage of the sparse matrix  $\mathbf{J}$  is set up by using a compressed sparse column (CSC) format. However, since the numerical inversion of  $\mathbf{J}$  is too costly, we have resorted to an incomplete  $LU$  factorization [3] and obtained an approximate inverse of  $\mathbf{J}$  to be inserted in Eq.(2). It is the use of this approximate inverse of  $\mathbf{J}$  that makes the procedure a quasi-Newton method instead of an ordinary Newton method. Specifically for our problem, this method proves to converge better than alternative versions of the quasi-Newton method (such as the SR1 or Broyden's methods [4]).

For a given trial value of  $\mu$ , we routinely perform 40 iterations for the discretized gap  $\vec{\Delta}$  according to Eq. (2). We then update the chemical potential  $\mu$  through a single step of the secant method applied to the number equation  $N = \int d\mathbf{r} n(\mathbf{r})$  at fixed  $\Delta(\mathbf{r})$ . With this new value of  $\mu$ , we again repeat 40 iterations for  $\vec{\Delta}$ , and so on. In the presence of a large number of vortices (about one hundred or more), 50 steps to update  $\mu$ , each followed by 40 iterations for  $\vec{\Delta}$ , are typically required to reach a satisfactory convergence. With a smaller number of vortices, on the other hand, these numbers can considerably be decreased (together with the number of points for the spatial grid in the  $xy$  plane). In order to speed up the calculation (and to make it feasible, in practice, for a large number of vortices), the coefficients  $\tilde{\mathcal{I}}_0(\mathbf{r})$  and  $\mathcal{I}_1(\mathbf{r})$  are calculated over an interpolation grid  $100 \times 100 \times 100$  in the variables ( $|\mathbf{A}|, |\Delta|, \bar{\mu} \equiv \mu - V(\mathbf{r})$ ), with a logarithmic spacing for  $\Delta$ . [Note that this grid is over the possible values of  $|\mathbf{A}|, |\Delta|$ , and  $\bar{\mu}$ , and not over the physical space spanned by the variable  $\mathbf{r}$ .] The values of the coefficients  $\tilde{\mathcal{I}}_0(\mathbf{r})$  and  $\mathcal{I}_1(\mathbf{r})$  at position  $\mathbf{r}$  are then obtained by a trilinear interpolation within a cube containing the point  $|\mathbf{A}(\mathbf{r})|, |\Delta(\mathbf{r})|$ , and  $\bar{\mu}(\mathbf{r})$ . In this way, the most demanding cases (like that shown in Fig. 1a of the main text) required 30 hours of CPU time on a standard desktop computer (with no parallelization of the code).

For frequencies close to  $\Omega_{c1}$ , where the solution with one vortex is almost degenerate with that without vortices, one needs to be particularly careful. In this case, we have used for the initial *ansatz* the product of the gap profile  $\Delta_{TF}(\mu - V(x, y, z))$  within a local density approximation for the system in the absence of rotation

[5] (where  $V(x, y, z)$  is the trapping potential), with the function

$$f(\mathbf{r}; \mathbf{R}_0) = \frac{x - X_0 + i(y - Y_0)}{\sqrt{\xi_0^2 + (x - X_0)^2 + (y - Y_0)^2}} \quad (3)$$

which simulates a vortex of radius  $\xi_0$  centered at  $\mathbf{R}_0 = (X_0, Y_0)$ . Here, the position and radius of the vortex are parameters that can be varied to optimize the solution. In particular, the initial position of the vortex should be slightly displaced from the trap center, to avoid the system being trapped in an excited state for  $\Omega < \Omega_{c1}$ . In this way, for  $\Omega > \Omega_{c1}$  (but still close to  $\Omega_{c1}$ ) the vortex adjusts its position and radius to the convergence values. For  $\Omega < \Omega_{c1}$ , on the other hand, the vortex migrates towards the edges of the cloud and eventually disappears.

At larger rotation frequencies, to speed up the calculations we have used as initial *ansatz* a gap profile given by the above local density approximation, but now multiplied by a triangular lattice of vortices which are spaced according to Feynman's theorem. Specifically, this is implemented by multiplying the gap profile  $\Delta_{TF}(\mu - V(x, y, z))$  within local density with the function  $\prod_{v=1}^{\mathcal{N}_v} f(\mathbf{r}; \mathbf{R}_v)$ , where  $f(\mathbf{r}; \mathbf{R}_v)$  is given by the expression (3) with  $\mathbf{R}_v = (X_v, Y_v)$  replacing  $\mathbf{R}_0 = (X_0, Y_0)$  and  $\xi_v$  replacing  $\xi_0$ ,  $\{(X_v, Y_v); v = 1, \dots, \mathcal{N}_v\}$  being the initial positions of  $\mathcal{N}_v$  vortices in a triangular lattice spaced according to Feynman's theorem. It turns out that this initial configuration contains about twice the number of vortices of the final configuration at convergence (since Feynman's theorem is progressively violated when approaching the border of the cloud). Correspondingly, the iteration procedure evolves in such a way that a number of vortices progressively evaporates away from the border of the cloud, until the system reaches its final equilibrium configuration. Quite generally, in the course of the iterations the radii of the vortex cores adjust to their convergence values rather quickly, while a larger number of iterations is required to reach convergence as far as the positions and number of vortices are concerned.

### Spontaneous self-assembling of vortex arrays

The distinct power of the present method is that vortex arrays can be generated through the cycles of self-consistency at a finite rotation frequency, even when the initial condition for the gap profile contains (essentially) no vortices. In this respect, during iterations we have found that, quite generally, vortices enter from the edges of the cloud and eventually reach their equilibrium positions inside the cloud.

As a demonstration of a typical numerical simulation that shows the evolution through the cycles of self-consistency, we report here a simplified version of the calculations presented in the main text, where now it is the chemical potential  $\mu$  and not the particle number  $N$  to be kept fixed at a given value through the cycles of self-consistency (in this case, we use thermodynamic value

$\mu = 0.752E_F$  of Fig. 3b of the main text). In addition, to speed up the calculation further we now utilize a spatial grid with  $300 \times 300 \times 35$  points instead of the denser one with  $500 \times 500 \times 50$  points used for the calculations in the main text for the trap of ref.[2].

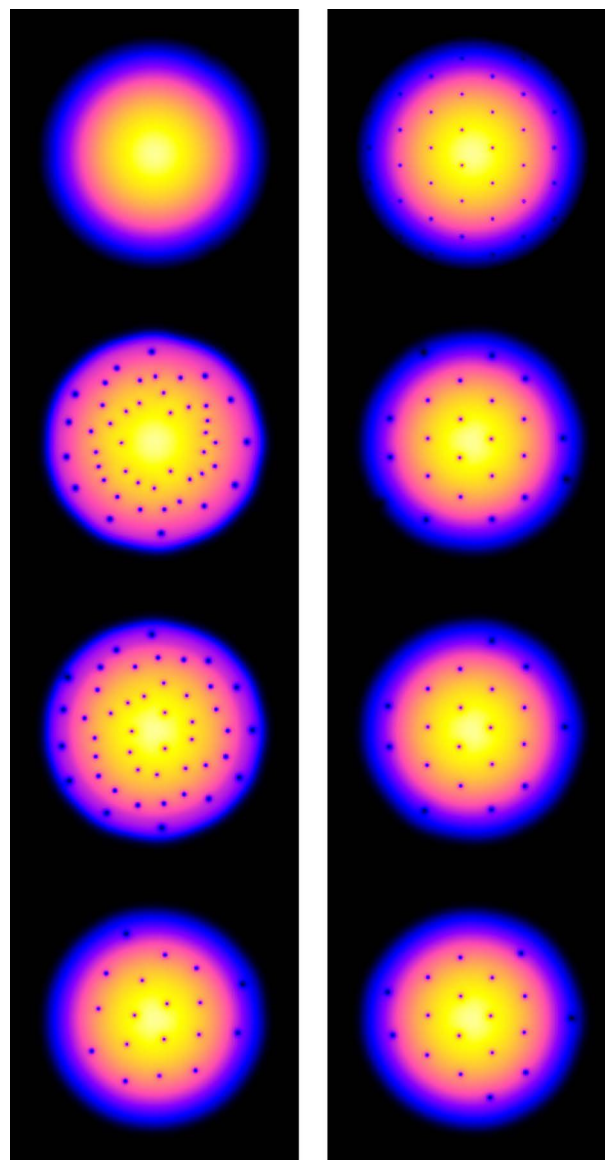


Figure S1. **The evolution of the gap profile through iterations.** The evolution of the gap profile in the course of the iterations is shown at unitarity,  $T = 0$ , and  $\Omega = 0.3\Omega_r$  for the trap parameters of ref. [2]. Left column (from top to bottom): initial configuration without vortices, and configurations after 400, 800, and 18000 iterations. Right column (from top to bottom): initial configuration with 37 vortices, and configurations after 400, 800, and 6000 iterations.

Figure S1 shows a typical evolution of the gap profile during the cycles of self-consistency for the trap of ref.[2] at unitarity, zero temperature, and  $\Omega = 0.3\Omega_r$ , using *two different initial configurations*: in the left column, a gap profile with no vortex but only a phase imprint

of equilateral triangular symmetry at the cloud edge; in the right column, a gap profile containing 37 vortices as required by Feynman's theorem. In order to reduce the distortion of the triangular lattice in the left column, the equilibrium value  $0.3\Omega_r$  has been reached only asymptotically in the course of the iteration cycles through a suitable damped saw-tooth profile of the angular frequency  $\Omega$  (a movie showing the complete evolution for this case is available at <http://bcsbec.df.unicam.it/?q=node/1>). The result is that these two quite different initial configurations lead essentially (apart from an overall rotation) to the same final solution at convergence with a total of 18 vortices (note also that the panel at the bottom of the right column of Fig. S1 coincides with Fig. 3b of the main text, the minor differences being ascribed to the different number of points in the spatial grids).

### The $\Omega$ vs $T$ phase diagram for the superfluid phase of a neutral trapped Fermi gas

It is interesting to combine together the two physical effects which yield a finite value for the moment of inertia in the superfluid phase, namely, the presence of: (i) An array of vortices even in the absence of a normal component when the angular frequency increases above a threshold, as occurs at zero temperature (cf. Fig. 3a of the main text); (ii) A normal component at finite temperature even in the absence of vortices, as occurs for vanishing angular frequency (cf. Fig. 4 of the main text). Simultaneous consideration of both effects leads us to construct a *phase diagram* for the temperature dependence of the lower critical frequency  $\Omega_{c1}$  about which the first vortex stably appears in the trap and of the upper critical frequency  $\Omega_{c2}$  about which the superfluid region disappears from the trap. This phase diagram is the analogue of that for a homogeneous type-II superconductor, showing the temperature dependence of the critical magnetic fields  $H_{c1}$  and  $H_{c2}$  [6].

The results of this calculation are reported in Fig. S2 at unitarity for the trap corresponding to the experiment of ref.[2]. More precisely, at a given temperature we have found it necessary to distinguish between a lower ( $l$ ) and an upper ( $u$ ) value for  $\Omega_{c1}$  and for  $\Omega_{c2}$  according to the following considerations. The lower value  $\Omega_{c1}^{(l)}$  corresponds to the smaller angular frequency  $\Omega$  at which an isolated vortex placed initially close to the trap center (say, at a distance  $R_s/10$  from it) begins to be attracted toward the trap center in the course of the cycles of the self-consistent solution of the LPDA equation. The upper value  $\Omega_{c1}^{(u)}$  corresponds instead to the smaller value of  $\Omega$  at which an isolated vortex placed initially at the edge  $R_s$  of the superfluid part of the cloud begins to be attracted toward the trap center. The ensuing uncertainty in the identification of  $\Omega_{c1}$ , which is unavoidably present for a trap with finite size, corresponds to the shaded red area of Fig. S2. On the other hand, the lower value  $\Omega_{c2}^{(l)}$

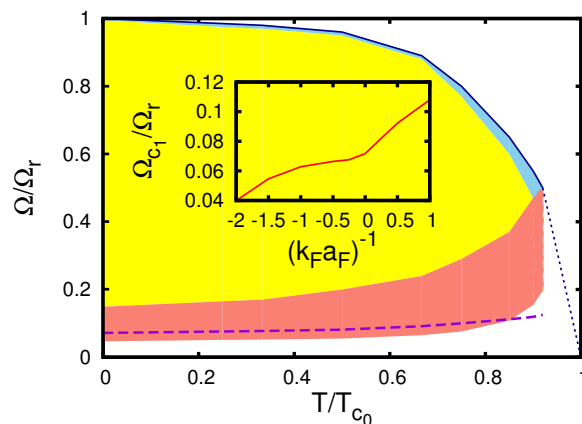


Figure S2. **Phase diagram for the critical frequencies  $\Omega_{c1}$  and  $\Omega_{c2}$  vs temperature.** Temperature dependence of the two critical frequencies  $\Omega_{c1}$  and  $\Omega_{c2}$  (in units of the radial trap frequency  $\Omega_r$ ) at unitarity for the trap of ref.[2]. The shaded red (blue) area corresponds to the uncertainty associated with  $\Omega_{c1}$  ( $\Omega_{c2}$ ). At a given temperature, no vortex is present for  $0 \leq \Omega < \Omega_{c1}^{(l)}$  while vortex arrays appear for  $\Omega_{c1}^{(u)} \leq \Omega < \Omega_{c2}^{(l)}$  (shaded yellow area). The broken line extrapolates the values of  $\Omega_{c2}^{(u)}$  down to the point ( $\Omega = 0, T = T_{c0}$ ), while the dashed line corresponds to Eq.(1) of the main text with appropriate (temperature dependent) values of  $\xi$  and  $R_s$ . The inset shows  $\Omega_{c1}$  at  $T = 0$  vs the coupling  $(k_F a_F)^{-1}$  again obtained from Eq.(1) of the main text with the appropriate values of  $\xi$  and  $R_s$  at zero temperature.

corresponds to the smaller value of  $\Omega$  at which all vortices have eventually disappeared from the trap, while the upper value  $\Omega_{c2}^{(u)}$  is determined by the condition that the gap parameter itself vanishes everywhere in the trap. [In this context, we have found that approaching  $\Omega_{c2}^{(u)}$ , the spatial width of  $\Delta(\mathbf{r})$  shrinks progressively but never becomes smaller than the size of the ground-state wave function of the harmonic trap, and that from this point on it is the height of  $\Delta(\mathbf{r})$  to decrease to zero.] The ensuing uncertainty in the identification of  $\Omega_{c2}$  corresponds to the shaded blue area of Fig. S2. For the specific trap and coupling conditions under which Fig. S2 was constructed, the values of  $\Omega_{c1}$  and  $\Omega_{c2}$  with their related uncertainties could be identified up to the maximum temperature  $0.92 T_{c0}$  where  $T_{c0}$  is the critical temperature in the trap for  $\Omega = 0$ . Finally, the shaded yellow area which extends from  $\Omega_{c1}^{(u)}$  to  $\Omega_{c2}^{(l)}$  is where arrays of vortices are present for given values of  $\Omega$  and  $T$ .

For comparison, the dashed line in Fig. S2 corresponds to the approximate expression (1) of the main text, in which we have inserted the appropriate (temperature-dependent) values of  $k_F \xi$  for an isolated vortex taken from ref.[7] and of  $k_F R_s$  obtained from the present calculation. It is remarkable that the curve obtained from the approximate expression (1) of the main text falls within the shaded red area of Fig. S2 obtained by the full nu-

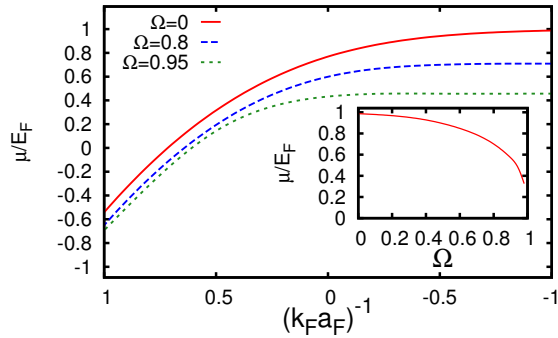


Figure S3. **Effect of rotation on the chemical potential.** Coupling dependence of the chemical potential in the trap (in units of  $E_F$ ) at  $T = 0$  for three different angular frequencies (in units of  $\Omega_r$ ). The inset shows the chemical potential vs  $\Omega$  for  $(k_F a_F)^{-1} = -1$ .

merical calculation. We have then used this approximate expression to get an estimate for the coupling dependence of  $\Omega_{c1}$  at zero temperature which is reported in the inset of Fig. S2. The values of  $\Omega_{c1}$  obtained in this way are in line with the sharp thresholds occurring in Fig. 3a of the main text, where, however, the numerical procedure sets these thresholds at the lower values of  $\Omega_{c1}^{(l)}$ .

### Chemical potential

It is interesting to determine the effect of a fast trap rotation also on the fermionic chemical potential, which is an essential ingredient of the BCS-BEC crossover. To this end, Fig. S3 shows the coupling dependence of the chemical potential  $\mu$  in the trap at zero temperature for several angular frequencies approaching the limiting value  $\Omega = \Omega_r$ , past which the fermion cloud is no longer bound. The rotation affects  $\mu$  more markedly on the BCS than on the BEC side of unitarity, the dependence becoming rather abrupt in the BCS limit as shown in the inset of Fig. S3 for  $(k_F a_F)^{-1} = -1$ .

### Fluctuation corrections emerging from an inhomogeneous mean-field approach

Quite generally, a mean-field calculation for an inhomogeneous situation (of the type dealt with by the BdG or LPDA equations) contains contributions from what are referred to as fluctuation corrections in a homogeneous situation. This is because, in an inhomogeneous situation, the imprint of the lowest excited states can be found in the ground-state wave function (as discussed, for instance, in ref.[8]). As an example, Fig. S4 reports a comparison of the coherence (healing) length of the gap parameter, obtained alternatively by solving the BdG equations for an isolated vortex (cf. ref.[7]) and by adding pairing (Gaussian) fluctuations on top of the homogeneous BCS mean field (cf. ref.[9]). This comparison shows that a BdG calculation is able to capture fluctuation contributions beyond mean field as far as the spatial variations of the gap parameter are concerned.

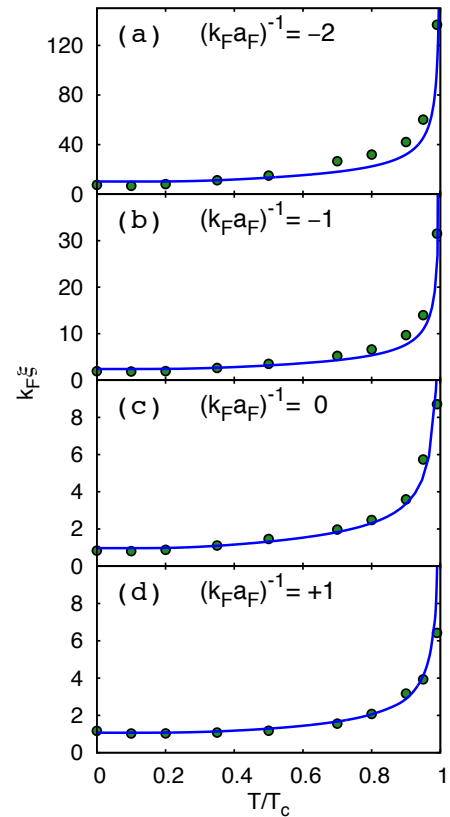


Figure S4. **Coherence length obtained by homogeneous mean field plus Gaussian fluctuations and by inhomogeneous mean field.** Comparison of the temperature dependence of the coherence length  $\xi$  (in units of  $k_F^{-1}$ ), obtained alternatively by including Gaussian fluctuations on top of the homogeneous BCS mean field (full lines) and by a numerical solution of the inhomogeneous BdG equations for an isolated vortex embedded in an infinite superfluid (dots), for different values of the coupling parameter  $(k_F a_F)^{-1}$ . The temperature is in units of the superfluid critical temperature  $T_c$  of the homogeneous system. The results of the homogeneous calculation have been rescaled by an overall factor of  $2/3$ , which takes into account the different definitions used for the same physical quantity by the two independent numerical calculations. [Figure adapted from Fig. 10 of ref.[9].]

In addition, as emphasized in the main text, the vortex profile (and thus the healing length) is not affected by the presence of the surrounding vortices, and the distance between two adjacent vortices is an order of magnitude larger than the healing length. Possible corrections to the healing length should thus have a minimal impact on the distribution of vortices.

Nor even the further inclusion of pairing fluctuations beyond the Gaussian ones is expected to change the vortex profile significantly. This is shown in Fig. S5, which compares the vortex profiles at unitarity and zero temperature, obtained alternatively by the BdG/LPDA ap-

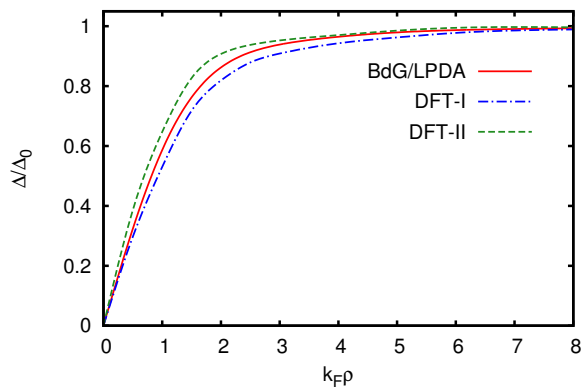


Figure S 5. **Effect of fluctuation corrections on the profile of an isolated vortex.** Comparison of the vortex profiles at unitarity and zero temperature, obtained by the BdG/LPDA approach (full line) and by the DFT approach (dashed-dotted and broken lines). The BdG/LPDA profile is taken from Fig. 1c of the main text, while the DFT profiles have been extracted from Fig. 2 of ref.[10] where two different parameterizations (I and II) were used for the DFT approach (referred to as the EDF approach in that reference).

proach (full line) and by the Density-Functional-Theory (DFT) approach of ref.[10] (dashed-dotted and broken lines) within two different parameterizations (referred to

as I and II). Rather remarkably, the BdG/LPDA profile just lies within the uncertainty of the DFT profiles in this important case [11].

- [1] M. W. Zwierlein, J. R. Abo-Shaeer, A. Schirotzek, C. H. Schunck, and W. Ketterle, *Nature* **435**, 1047 (2005).
- [2] S. Riedl, E. R. Sánchez Guajardo, C. Kohstall, J. Hecker-Denschlag, and R. Grimm, *New J. Phys.* **13**, 035003 (2011).
- [3] C. G. Broyden and M. T. Vespucci, *Krylov Solvers for Linear Algebraic Systems* (Elsevier B.V., Amsterdam, 2004).
- [4] J. Nocedal and S. J. Wright, *Numerical Optimization* (Springer Science, New York, 1999).
- [5] A. Perali, P. Pieri, and G. C. Strinati, *Phys. Rev. A* **68**, 031601 (2003).
- [6] P. G. de Gennes, *Superconductivity of Metals and Alloys* (Benjamin, New York, 1966).
- [7] S. Simonucci, P. Pieri, and G. C. Strinati, *Phys. Rev. B* **87**, 214507 (2013).
- [8] E. P. Gross, *J. Math. Phys.* **4**, 195 (1963).
- [9] F. Palestini and G. C. Strinati, *Phys. Rev. B* **89**, 224508 (2014).
- [10] A. Bulgac and Y. Yu, *Phys. Rev. Lett.* **91**, 190404 (2003).
- [11] At unitarity, the profile of an isolated vortex obtained by the LPDA approach coincides at any temperature with that obtained by the BdG approach, as shown in Fig. 2 of ref.[12].
- [12] S. Simonucci and G. C. Strinati, *Phys. Rev. B* **89**, 054511 (2014).